

Electric impedance microflow cytometry for characterization of cell disease states†

Cite this: *Lab Chip*, 2013, 13, 3903

E. Du,^{‡a} Sungjae Ha,^{‡b} Monica Diez-Silva,^a Ming Dao,^{*a} Subra Suresh^c and Anantha P. Chandrakasan^{*b}

The electrical properties of biological cells have connections to their pathological states. Here we present an electric impedance microflow cytometry (EIMC) platform for the characterization of disease states of single cells. This platform entails a microfluidic device for a label-free and non-invasive cell-counting assay through electric impedance sensing. We identified a dimensionless offset parameter δ obtained as a linear combination of a normalized phase shift and a normalized magnitude shift in electric impedance to differentiate cells on the basis of their pathological states. This paper discusses a representative case study on red blood cells (RBCs) invaded by the malaria parasite *Plasmodium falciparum*. Invasion by *P. falciparum* induces physical and biochemical changes on the host cells throughout a 48-h multi-stage life cycle within the RBC. As a consequence, it also induces progressive changes in electrical properties of the host cells. We demonstrate that the EIMC system in combination with data analysis involving the new offset parameter allows differentiation of *P. falciparum* infected RBCs from uninfected RBCs as well as among different *P. falciparum* intraerythrocytic asexual stages including the ring stage. The representative results provided here also point to the potential of the proposed experimental and analysis platform as a valuable tool for non-invasive diagnostics of a wide variety of disease states and for cell separation.

Received 1st May 2013,
Accepted 12th July 2013

DOI: 10.1039/c3lc50540e

www.rsc.org/loc

Introduction

Electric impedance spectroscopy (EIS) is a well established technique and has been widely utilized in the development of various biosensors.¹ This method offers a complementary technique for *in vivo* detection of a variety of cancers including malignancy in the liver,² bladder,³ skin⁴ and breast.⁵ For *in vivo* EIS-based detection, the detectability and spatial resolution of lesions are highly limited by the contrast ratio of the focal region and its surroundings.⁶ The electric impedance (EI) of the malignant tissues measured by EIS is relatively lower compared to those of normal tissues over radio frequency range.

Similarly, at the cellular level, variation in electrical properties of cells may be linked to the biochemical changes introduced by disease pathology. This variation can be detected through EI sensing of cell-substrate interactions,

which was initiated by Giaever and Keese in 1984.⁷ This method has been widely utilized to monitor cellular response to various stimuli, such as drug treatment,⁸ infection by the malaria parasite,^{9,10} and proliferation of leukaemia cells,¹¹ and to detect molecular or cell bounding events (through interactions of antibody-antigens, proteins, enzymes, *etc.*) such as those involving the influenza virus¹² and breast cancer cells.¹³ This method usually requires immobilization of a bio-recognition element on the surface of sensing electrodes or detection sites for enhanced specificity and signal amplification. Further recent developments include single-cell EI sensing systems utilizing microfluidic flow control in combination with microfabricated electrode structures,^{14–16} which ensures high detection sensitivity as variations in electric current flow induced by the perturbation from cellular presence or biochemical interactions occurs adjacent to sensing electrodes. Single-cell EI has been demonstrated to be an effective strategy for cell counting,¹⁷ discrimination of various cell lines such as monocytes from dendritic cells and fibroblasts from adipocytes,¹⁸ and detection of *Babesia bovis*-infected bovine red blood cells (RBCs).¹⁹ Systematic modelling and simulation of the single-cell EI was conducted to link the dielectric properties to the cellular impedance response.²⁰ For parasitic diseases, EI sensing relies on the changes in electrical properties of the cytoplasm and cell membrane, as the variation resulting from size changes of infected cells is negligible.

^aDepartment of Materials Science and Engineering, Massachusetts Institute of Technology, 77 Massachusetts Avenue, Cambridge, MA 02139, USA.
E-mail: mingdao@mit.edu

^bDepartment of Electrical Engineering and Computer Science, Massachusetts Institute of Technology, 77 Massachusetts Avenue, Cambridge, MA 02139, USA.
E-mail: anantha@mit.edu

^cDepartment of Materials Science and Engineering and Department of Biomedical Engineering, Carnegie Mellon University, Pittsburgh, PA 15213, USA

† Electronic supplementary information (ESI) available. See DOI: 10.1039/c3lc50540e

‡ These authors contributed equally to this work.

Diagnosis of malaria, an infectious disease threatening human health, relies on the detection and counting of infected red blood cells (iRBCs). There were an estimated 216 million episodes of malaria and an estimated 655 000 malaria deaths in 2010, of which 91% were in Africa.²¹ Among five types of *Plasmodium* infecting humans, *Plasmodium falciparum* is the deadliest strain causing malaria.²² *P. falciparum* infection not only alters the membrane permeability of the host RBCs for nutrient uptake and waste disposal but also consumes RBC hemoglobin forming hemozoin crystals.²³ Associated with these biochemical changes, the host RBCs undergo biophysical modifications of electrical,¹⁰ optical,²⁴ mechanical,^{24,25} and magnetic²⁶ properties. The first application of EI measurement in physiological characterization for *P. falciparum* iRBCs (*Pf*-iRBCs) was performed using the cell-substrate interaction sensing.¹⁰ The measurement was performed at the late intra-erythrocytic development stage. It also relied on a special method to trap RBCs based on antigen/antibody cross-linking and a self-assembled monolayer thus significantly limiting test throughputs. A recent work on single cell EI detection of mature stage *Pf*-iRBCs was realized based on conductance changes and characteristic dwell time using a graphene transistor integrated in a microfluidic channel.²⁷ The sensing was carried out in a “flow-catch-release” mode *via* bio-recognition protein functionalization on the graphene surface. Still, a high throughput (continuous flow detection) and high sensitivity diagnostic method for detecting *P. falciparum* infection, especially the intraerythrocytic asexual ring stage, is necessary for field diagnostic tests and such a method is currently not available.

In this paper, we demonstrate an electric impedance microflow cytometry (EIMC) platform for reliable differentiation of each intraerythrocytic asexual stage of *Pf*-iRBCs. The EIMC platform is featured with continuous blood flow measurement without any cell immobilization treatment, target labelling, or electrode modification using bio-recognition elements. The performance of the EIMC system was tested with *Pf*-iRBCs. We considered both components of EI measurement of *Pf*-iRBCs, *i.e.* magnitude and phase, to establish a novel evaluation parameter for discrimination of different disease states.

Materials and methods

P. falciparum culture and sample preparation

P. falciparum was cultured in leukocyte-free human RBCs (Research Blood Components, Brighton, MA) under an atmosphere of 5% CO₂ balanced with N₂, at 5% hematocrit in RPMI culture medium 1640 (Gibco Life Technologies) supplemented with 25 mM HEPES (Sigma), 200 mM hypoxanthine (Sigma), 0.20% NaHCO₃ (Sigma) and 0.25% Albumax II (Gibco Life Technologies). The cultured *P. falciparum* sample prior to EIMC measurement consisted of a mixture of multi-stage *Pf*-iRBCs and uninfected RBCs at parasitemia of 5% to 8%.

The working solution for EI measurement was phosphate-buffered saline (PBS; 2.67 mmol l⁻¹ KCl, 1.47 mmol l⁻¹ KH₂PO₄,

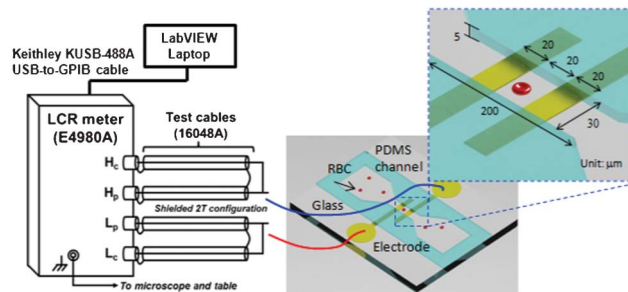


Fig. 1 Experimental EIMC system setup for *Pf*-iRBC detection using a microfluidic device.

137.93 mmol l⁻¹ NaCl, 8.06 mmol l⁻¹ Na₂HPO₄·7H₂O) mixed with Bovine Serum Albumin (BSA) (Sigma-Aldrich, St Louis, MO) to maintain osmotic pressure and prevent RBC adhesion to the microfluidic channel. Three concentrations of BSA-PBS, 0.2%, 0.5%, and 1% weight/volume (w/v) were utilized in the experiments to achieve optimum performance and sensitivity of EI measurements. The cultured *P. falciparum* samples were cooled down to room temperature after being removed from the incubator, then washed with PBS solution at 2000 rpm for 5 min at 21 °C and diluted by 200 times in the working solution.

Microfluidic EIMC system

The experimental setup for EI measurement is shown in Fig. 1. The proposed microfluidic device for EI measurement consists of a microfluidic channel integrated with Ti/Au electrodes. The Ti/Au electrode of 10 nm/100 nm thickness was deposited on a thin glass substrate (500 μm) using E-beam vaporization and standard microfabrication techniques. The microfluidic channel was fabricated using poly (dimethylsiloxane) PDMS casting protocols and bonded to the glass substrate. The two electrodes were 20 μm wide with 20 μm spacing embedded in the narrowest portion of the microfluidic channel (30 μm × 5 μm cross-sectional area) to probe individual human RBCs. The microfluidic EIMC system exhibited excellent optical qualities, allowing direct observation *via* microscopy. Measurements were performed on an Olympus IX 71 inverted microscope using a halogen source (100 W). Identification of *Pf*-iRBCs and specific stage was achieved using a long working distance lens with 100× magnification and numerical aperture NA = 0.8 (Olympus LMPLFLN100X). The electrodes were connected with an E4980A precision LCR meter (Agilent Technology, Inc.) for EI measurement. Communication between the LCR meter and data-recording computer was realized through a Keithley KUSB-488A USB-to-GPIB cable. To reduce the error due to stray capacitance, the wires were connected in a shielded two-terminal configuration. Lab-VIEW software (National Instruments Corp., Austin, TX) was used for automatic data acquisition.

The biochemical alterations during the multi-stage life cycle of *P. falciparum* lead to corresponding transitions in electrical properties of the host RBCs. As indicated by the equivalent circuit model of single *Pf*-iRBC suspended between two electrodes (see Fig. S1(b), ESI† similar to the classic circuit model of single cells),^{1,20} the cell membrane capacitance

shields the cell interior from the external electric field at low frequencies. At higher frequencies, owing to the short-circuiting effect of membrane capacitance, the electric field penetrates to the cellular interior and reaches the parasite. The present EI measurements were performed under a single frequency of 2 MHz with a sampling rate of 50 Hz in order to probe both interfacial and intracellular changes of *Pf*-iRBCs. The frequency falls into the β dispersion regime (usually within the range 0.1–10 MHz)²⁸ where the large discrepancy in conductivity of the cellular membrane and cytoplasm causes a lag in charging response of the intracellular and extracellular substances. A continuous steady flow of evenly distributed cell suspension was generated by an exterior pressure gradient from two water columns, allowing minimum hydrodynamic disturbance during EI measurement while maintaining sufficient signal sampling. A stream of individual cells is managed where cells cross over electrodes with minimum bias from the midstream in order to maintain a steady detection signal.

Results

The proposed EIMC system possesses a cell-counting function. When a cell approaches and crosses the electrodes, the presence of the cell at the measuring zone forms a lossy capacitor, creating a dynamic impedance transition ΔZ from the base impedance of the system. The EI transition is given by,

$$\Delta Z = Z_{s+Pf-iRBC} - Z_s \approx -Z_s^2 / (Z_s + Z_{Pf-iRBC}) \quad (1)$$

which is a complex function of cellular impedance $Z_{Pf-iRBC}$ and medium impedance Z_s with the effects from the electric double layer (EDL) at the medium-electrode interfaces excluded (see Fig. S1(c) ESI†). The magnitude deviation ΔM and the phase deviation $\Delta\phi$ are taken from the peaks of each ΔZ transition, and they are complex functions of cell size, composition, dielectric properties of the cytoplasm and the cell membrane, and the enclosure of the medium surrounding the cell.

Fig. 2 shows a typical example of EI transitions measured when cells cross the electrodes (see Table S1 ESI† for EI transition statistics). Magnitude and phase changes, ΔM and $\Delta\phi$, are shown in two subplots. The insert in the phase change subplot displays a representative image for each sub-population, from uninfected RBCs to ring stage, trophozoite stage, and schizont stage.

In order to systematically evaluate different experimental conditions, EI transitions were normalized separately by,

$$x = \Delta\phi / \overline{\Delta\phi} \quad (2)$$

$$y = \Delta M / \overline{\Delta M} \quad (3)$$

where $\overline{\Delta M}$ and $\overline{\Delta\phi}$ are the mean values of the magnitude change and the phase change of 120 uninfected RBCs for each corresponding BSA concentration (see Table S1 ESI†).

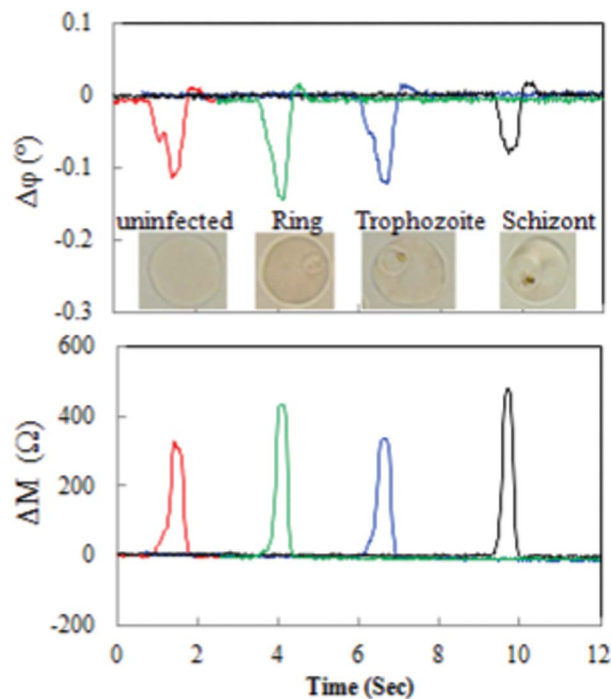


Fig. 2 EI transitions measured as uninfected RBCs and *Pf*-iRBCs crossed over the electrode probe. Measurement conditions: 2 MHz 1 V and 0.2% w/v BSA-PBS.

Detection of *Pf*-iRBCs was possible but limited based on either one of the normalized EI components in isolation. For 0.2% w/v BSA-PBS as demonstrated in Fig. 3, the normalized magnitude transition monotonically increases with the progressive malaria infection stages. The trend was not observed in normalized phase transition. Additionally, for higher BSA concentration conditions (0.5% w/v and 1% w/v), no consistent trends were found in either of the two normalized EI components as demonstrated in Fig. S2 and S3 ESI†. Fig. 3 shows statistically significant differences ($P < 0.001$) in normalized EI magnitude between all three stages of *Pf*-iRBCs and uninfected RBCs, although no significant differences can be found between adjacent *Pf*-iRBC stages.

In order to improve the disease state differentiation, we have established a new composite evaluation parameter to detect *Pf*-iRBCs at different stages. As Fig. 4(a) shows, the normalized EI components of uninfected RBCs at each BSA concentration can be well-fitted with linear curves as indicated by solid lines in the scatter plot. In Fig. 4(b), ring stage *Pf*-iRBCs are located in a slightly higher magnitude-phase region than the uninfected ones, and the late trophozoite and schizont *Pf*-iRBCs are obviously away from the other populations. In order to quantify this separation, we introduced a new dimensionless parameter, EI offset δ , as the distance from each data point to the reference line,

$$\delta = -(kx_n + a - y_n) / \sqrt{k^2 + a^2} \quad (4)$$

where k and a are the linear interpolation coefficients of the normalized impedance transitions of uninfected RBCs; x_n and

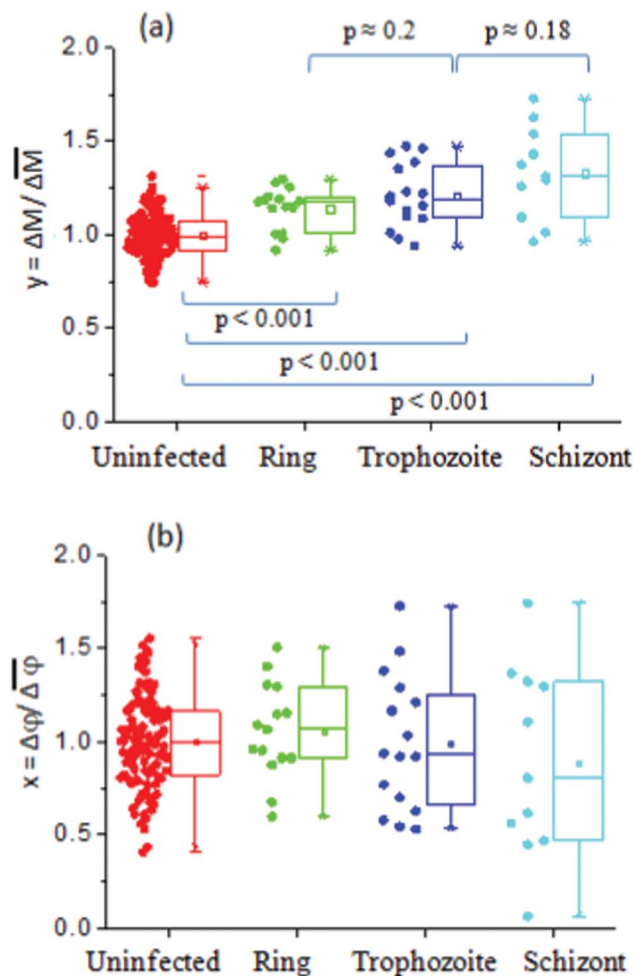


Fig. 3 (a) Scatter plot of normalized magnitude transition for uninfected RBCs and *Pf*-iRBCs in 0.2% w/v BSA-PBS. (b) Scatter plot of normalized phase transition for uninfected RBCs and *Pf*-iRBCs in 0.2% w/v BSA-PBS.

y_n are the normalized impedance transitions of individual RBCs. Although the normalized EI transitions varied between different experiments due to slight variations in sample and device preparation, a similar scatter pattern was observed. To combine data from each experiment, the scatter plots of EI transitions for *Pf*-iRBCs at various stages were aligned to have a common uninfected RBC reference line.

EI offsets δ for various *Pf*-iRBC stages were compared to the uninfected RBCs using statistical box charts for different BSA concentrations, shown in Fig. 5. The statistical analysis was carried out using a two-sample t-test (see Tables S2–S4 ESI†). When BSA concentration was 0.2% w/v, all intraerythrocytic stages of *Pf*-iRBCs showed a statistically significant difference ($P < 0.001$), as indicated in Fig. 5(a). With a small increase of BSA concentration to 0.5% w/v, all stages of *Pf*-iRBCs were still statistically different ($P < 0.001$). When BSA concentration increases further to 1% w/v, the ring stage bears moderate statistical significance ($P = 0.134$) despite trophozoite and schizont stages still having high statistical significance ($P < 0.001$). It is clear that the offset δ is more scattered at higher

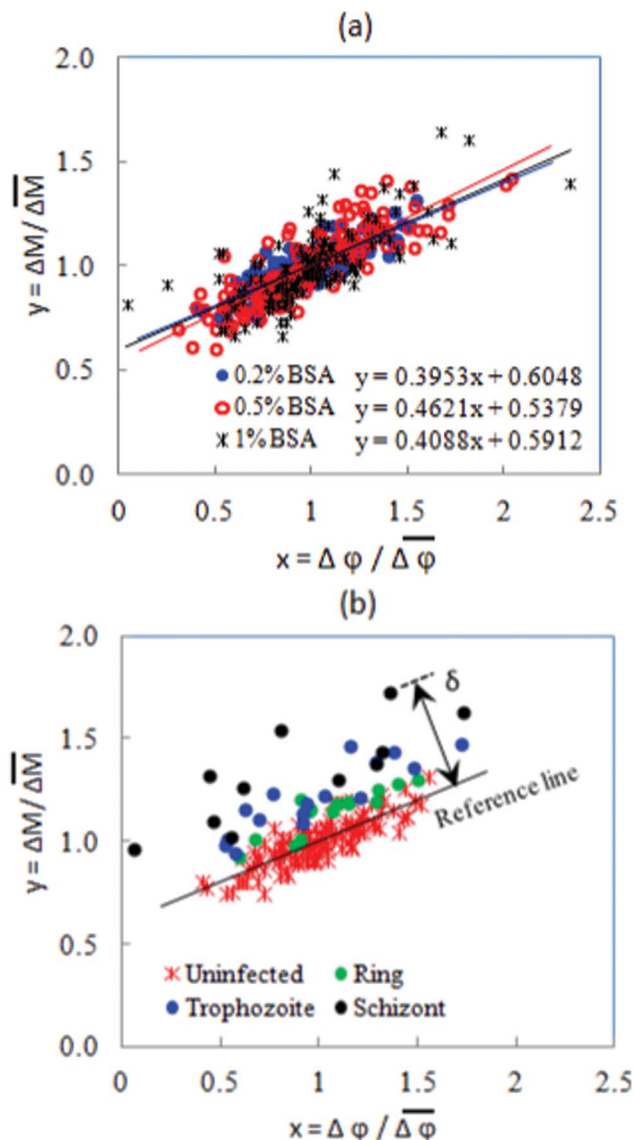


Fig. 4 (a) Scatter plot of normalized EI transitions of uninfected RBCs. (b) Scatter plot of normalized EI transitions for uninfected RBCs and *Pf*-iRBCs in 0.2% BSA-PBS and definition of Offset δ .

BSA concentrations. In addition, the overlap between uninfected RBCs and *Pf*-iRBCs, especially for ring and trophozoite stages increases with BSA concentration. As shown in Fig. 5(a), we also found that, at 0.2% w/v, our new EI measurement method can be used to effectively distinguish *Pf*-iRBCs between adjacent asexual stages (trophozoite vs. ring, and schizont vs. trophozoite) with high statistical significance.

Discussion

One of the major challenges in non-invasive malaria diagnostics has been the lack of effective differentiation strategy of early-stage *Pf*-iRBCs from uninfected RBCs. With the careful exploration of the optimum differentiation conditions, as

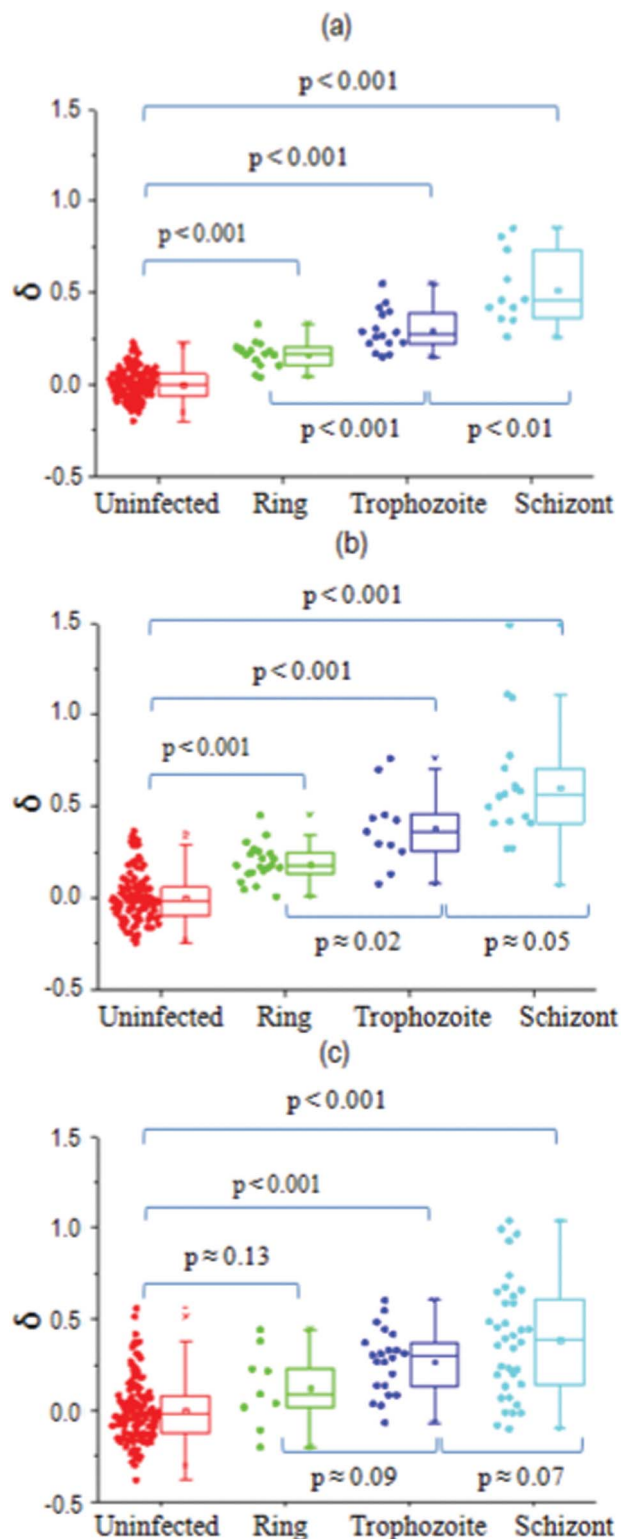


Fig. 5 Uninfected RBCs and *Pf*-iRBCs separation results in (a) 0.2% w/v BSA-PBS, (b) 0.5% w/v BSA-PBS, and (c) 1% w/v BSA-PBS.

shown in Fig. 3(a), using 0.2% w/v BSA-PBS, a statistically significant difference can now be found between ring stage *Pf*-iRBCs and uninfected RBCs, which had not been achieved in earlier studies using EI measurements.^{10,27}

We also recognized that BSA concentration may play an important role in the separation of *Pf*-iRBCs from uninfected RBCs. *Pf*-iRBCs at mature stages (trophozoite and schizont) have elevated expression of membrane proteins [*Pf*EMP]-1, forming surface protrusions or “knobs,”²⁹ which bear a positive charge (+20 mV) as indicated by Surface Potential Spectroscopy.³⁰ The difference in the magnitude of EI transitions decreases with BSA concentration among various *Pf*-iRBC stages. This suggests that adsorption of negatively charged BSA³¹ on the membrane of RBCs negates the surface charge modification associated with “knobs.” As a consequence, the inherent difference in surface charge density between different *Pf*-iRBC stages is likely to be minimized. This finding suggests that the lowest BSA concentration we tested, 0.2% w/v, was an optimum condition of the present EIMC system for *P. falciparum* diagnostic purposes while maintaining continuous flow of cells. A lower BSA concentration than 0.2% w/v may result in adhesion of cells to the channel walls and consequently ineffective or even impossible EI data collection.

Using the new parameter, EI offset δ , we have demonstrated significantly improved resolution and effectiveness in the detection of *Pf*-iRBCs and among various intraerythrocytic asexual stages using single frequency excitation. The consistent linear interpolation between the normalized magnitude and phase transitions of uninfected RBCs establishes a reliable base line. This reference line is carefully chosen to be the mean trend of the measurements from uninfected cells; however, it can be the mean trend from the entire population at field diagnostic applications since the uninfected RBC population is often dominant (>90%), even in severe malaria cases.³²

Studies of cell impedance have enabled a possible label-free diagnostic test by recourse to the measurement of specific parameters.³³ However, systematic demonstration of the evolution of cell pathological states has thus far not been reported. Indeed, accurate measurements of biophysical properties of a cell in a microfluidic device is usually limited by such factors as the high impedance of probe electrodes, stray capacitance, and electric double layer capacitance. In addition, the presence of the intra-erythrocytic parasite also alters the progressive evolution of the electric response of the cell.

In this paper, we have overcome these limitations by establishing a new parameter, EI offset δ , which contains both magnitude and phase information of the entire cell suspended in the medium. This parameter appears to provide a promising new marker for identifying the onset and progression of disease states at the cell level. By properly accounting for both EI magnitude and phase information, the single offset parameter enables the identification of progressive changes in the pathological state of a *Pf*-iRBC. The improved detectability of the subtle differences between ring-stage *Pf*-iRBCs and uninfected RBCs suggests that the EIMC system presented in this study may be adapted for improving disease state differentiation of different cell populations and other disease

classes involving electrical property changes. Sick cell anemia and acidosis are among the factors that are likely to have changes in EI properties of RBCs, and would be interesting topics of future systematic studies. By using the changes in the electrical signature to identify the evolution of cell disease states, the present method provides an additional tool to recent advances whereby changes in the mechanical signature^{34,35} or membrane flickering²⁴ have been linked as markers to detect cell disease states. To advance the state of the art and overcome any remaining limitations, more systematic efforts need to be carried out for practical medical applications.

Conclusion

The proposed microfluidic EIMC system provides a non-invasive and reliable detection method for *P. falciparum* infection. The detection of *P. falciparum* ring stage iRBCs in 0.2% BSA-PBS medium was achieved using normalized EI magnitude. Furthermore, with a newly developed dimensionless parameter, EI offset δ , the ring-stage Pf-iRBC detection was significantly improved. Statistically significant differentiation of Pf-iRBCs was also achieved between adjacent intraerythrocytic stages (trophozoite vs. ring, and schizont vs. trophozoite). The sensitivity of the Pf-iRBC detection and EIMC performance were found to be significantly influenced by BSA concentration and a number of other relevant factors, such as cell concentration, flow rate and sampling rate. The results indicate that 0.2% w/v BSA in PBS is optimum for the present EIMC measurements with sufficient detection sensitivity while minimizing cell adhesion to the microfluidic channel. The newly developed method using the composite parameter δ , instead of the single EI component approach in an approximated circuit model, is also expected to be broadly applicable in differentiating other types of diseased cells for disease diagnostics and cell separation.

Acknowledgements

Sungjae Ha acknowledges Fulbright Science and Technology Award. We thank S. J. Kim and J. Han for help in the initial system development and discussion in background experimental work. Device fabrications were carried out at MIT Microsystems Technology Laboratories. The authors acknowledge support by the National Research Foundation (Singapore) through Singapore-MIT Alliance for Research and Technology (SMART) Center (ID IRG), Singapore-MIT Alliance (SMA), MIT Center for Integrated Circuits and Systems (CICS), and the U. S. National Institutes of Health (Grant R01 HL094270).

References

1 R. Pethig and D. B. Kell, *Phys. Med. Biol.*, 1987, **32**, 933–970.

- 2 A. P. O'Rourke, M. Lazebnik, J. M. Bertram, M. C. Converse, S. C. Hagness, J. G. Webster and D. M. Mahvi, *Phys. Med. Biol.*, 2007, **52**, 4707–4719.
- 3 A. Keshtkar, A. Keshtkar and R. H. Smallwood, *Physiol. Meas.*, 2006, **27**, 585–596.
- 4 Y. A. Glickman, O. Filo, M. David, A. Yayon, M. Topaz, B. Zamir, A. Ginzburg, D. Rozenman and G. Kenan, *Skin Res. Technol.*, 2003, **9**, 262–268.
- 5 A. Malich, T. Bohm, M. Facius, I. Kleinteich, M. Fleck, D. Sauner, R. Anderson and W. A. Kaiser, *Nucl. Instrum. Methods Phys. Res., Sect. A*, 2003, **497**, 75–81.
- 6 A. Malich, M. Facius, R. Anderson, J. Bottcher, D. Sauner, A. Hansch, C. Marx, A. Petrovitch, S. Pflaiderer and W. Kaiser, *Eur. Radiol.*, 2003, **13**, 2441–2446.
- 7 I. Giaever and C. R. Keese, *Proc. Natl. Acad. Sci. U. S. A.*, 1984, **81**, 3761–3764.
- 8 F. Asphahani, K. Wang, M. Thein, O. Veiseh, S. Yung, J. A. Xu and M. Q. Zhang, *Phys Biol*, 2011, **8**.
- 9 A. K. Tripathi, D. J. Sullivan and M. F. Stins, *J. Infect. Dis.*, 2007, **195**, 942–950.
- 10 C. Ribaut, K. Reybier, O. Reynes, J. Launay, A. Valentin, P. L. Fabre and F. Nepveu, *Biosens. Bioelectron.*, 2009, **24**, 2721–2725.
- 11 C. Hao, F. Yan, L. Ding, Y. D. Xue and H. X. Ju, *Electrochem. Commun.*, 2007, **9**, 1359–1364.
- 12 C. A. Meseko, A. T. Oladokun, P. S. Ekong, F. O. Fasina, I. A. Shittu, L. K. Sulaiman, A. N. Egbuji, P. Solomon, H. G. Ularumu and T. M. Joannis, *Diagn. Microbiol. Infect. Dis.*, 2010, **68**, 163–165.
- 13 V. Srinivasaraghavan, J. Strobl and M. Agah, *Lab Chip*, 2012, **12**, 5168–5179.
- 14 H. E. Ayliffe, A. B. Frazier and R. D. Rabbitt, *J. Microelectromech. Syst.*, 1999, **8**, 50–57.
- 15 D. Malleo, J. T. Nevill, L. P. Lee and H. Morgan, *Microfluid. Nanofluid.*, 2010, **9**, 191–198.
- 16 M. H. Wang, M. F. Kao and L. S. Jang, *Rev Sci Instrum*, 2011, **82**.
- 17 L. L. Sohn, O. A. Saleh, G. R. Facer, A. J. Beavis, R. S. Allan and D. A. Notterman, *Proc. Natl. Acad. Sci. U. S. A.*, 2000, **97**, 10687–10690.
- 18 G. Schade-Kampmann, A. Huwiler, M. Hebeisen, T. Hessler and M. Di Berardino, *Cell Proliferation*, 2008, **41**, 830–840.
- 19 A. Valero, T. Braschler and P. Renaud, *Lab Chip*, 2010, **10**, 2216–2225.
- 20 H. Morgan, T. Sun, D. Holmes, S. Gawad and N. G. Green, *J. Phys. D: Appl. Phys.*, 2007, **40**, 61–70.
- 21 *World Malaria Report 2010*, World Health Organization, Geneva, 2010, 1–204.
- 22 A. M. Dondorp, E. Pongponratn and N. J. White, *Acta Trop.*, 2004, **89**, 309–317.
- 23 I. W. Sherman, *Microbiol Rev*, 1979, **43**, 453–495.
- 24 Y. K. Park, M. Diez-Silva, G. Popescu, G. Lykotrafitis, W. S. Choi, M. S. Feld and S. Suresh, *Proc. Natl. Acad. Sci. U. S. A.*, 2008, **105**, 13730–13735.
- 25 H. Bow, I. V. Pivkin, M. Diez-Silva, S. J. Goldfless, M. Dao, J. C. Niles, S. Suresh and J. Y. Han, *Lab Chip*, 2011, **11**, 1065–1073.
- 26 S. Hackett, J. Hamzah, T. M. E. Davis and T. G. St Pierre, *Biochim. Biophys. Acta, Mol. Basis Dis.*, 2009, **1792**, 93–99.

- 27 P. K. Ang, A. Li, M. Jaiswal, Y. Wang, H. W. Hou, J. T. L. Thong, C. T. Lim and K. P. Loh, *Nano Lett.*, 2011, **11**, 5240–5246.
- 28 H. P. Schwan, *Med Prog Technol*, 1993, **19**, 163–165.
- 29 M. Aikawa, K. Kamanura, S. Shiraishi, Y. Matsumoto, H. Arwati, M. Torii, Y. Ito, T. Takeuchi and B. Tandler, *Exp. Parasitol.*, 1996, **84**, 339–343.
- 30 J. Gruenberg, D. R. Allred and I. W. Sherman, *J. Cell Biol.*, 1983, **97**, 795–802.
- 31 U. Bohme and U. Scheler, *Chem. Phys. Lett.*, 2007, **435**, 342–345.
- 32 T. Hanscheid, *Clin. Lab. Haematol.*, 1999, **21**, 235–245.
- 33 T. Sun and H. Morgan, *Microfluid. Nanofluid.*, 2010, **8**, 423–443.
- 34 S. Suresh, *Acta Biomater.*, 2007, **3**, 413–438.
- 35 S. Suresh, J. Spatz, J. P. Mills, A. Micoulet, M. Dao, C. T. Lim, M. Beil and T. Seufferlein, *Acta Biomater.*, 2005, **1**, 15–30.

Electronic Supplementary Information

Electric Impedance Microflow Cytometry for Disease-State Characterization and Diagnostics†

E Du^{‡a}, Sungjae Ha^{‡b}, Monica Diez-Silva^a, Ming Dao^{*a}, Subra Suresh^a, Anantha P. Chandrakasan^{*b}

^a Department of Materials Science and Engineering, Massachusetts Institute of Technology, 77 Massachusetts Avenue., Cambridge, MA 02139, USA;
E-mail: mingdao@mit.edu

^b Department of Electrical Engineering and Computer Science, Massachusetts Institute of Technology, 77 Massachusetts Avenue., Cambridge, MA 02139, USA;
E-mail: anantha@mit.edu

‡ These authors contributed equally to this work.

Supplementary Figures

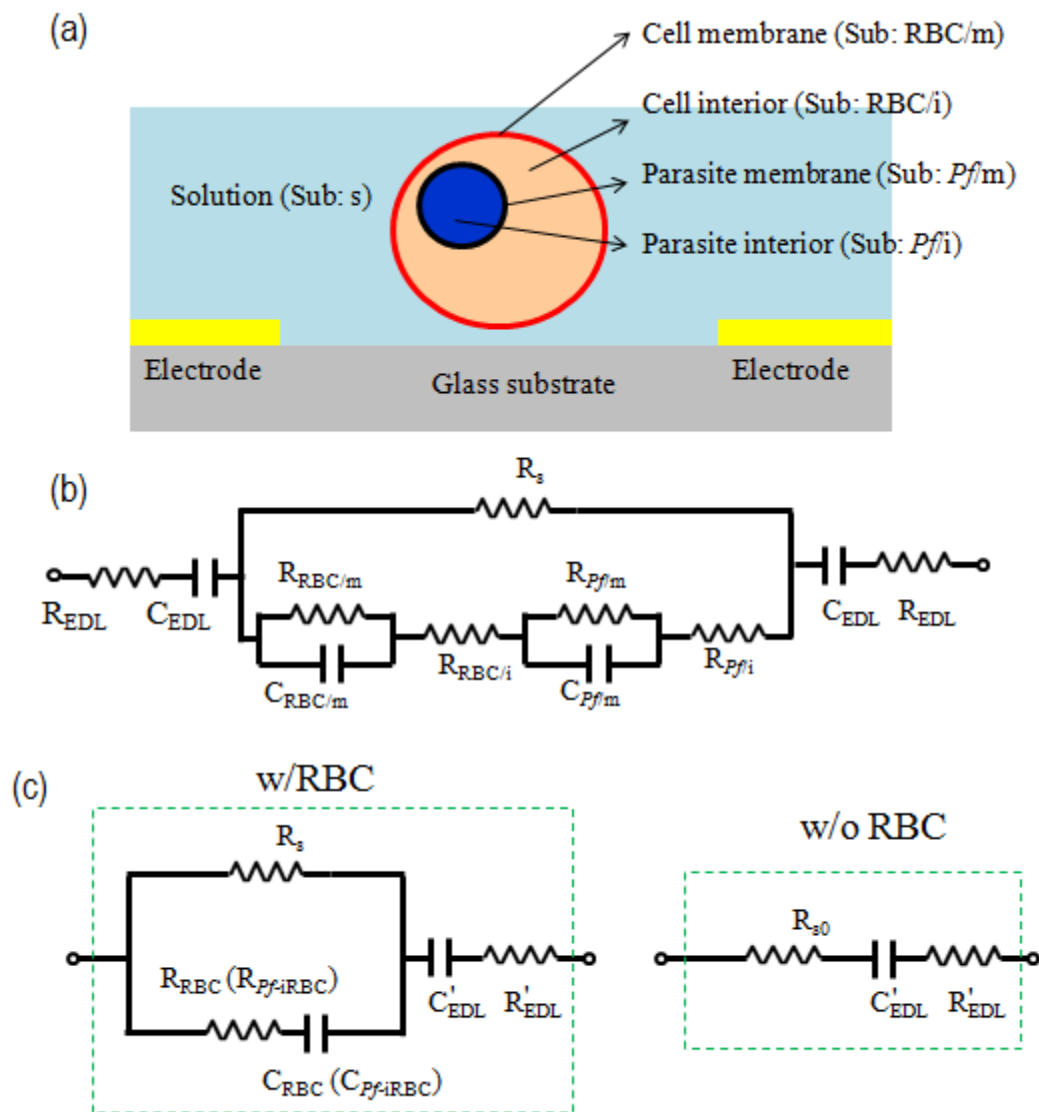


Fig.S1 (a) Schematic of a *Pf*-iRBC suspended in solution between two electrodes. (b) Equivalent complete circuit model of single *Pf*-iRBC suspended between two electrodes. (c) Unitary circuit model of single *Pf*-iRBC suspended between two electrodes (assume the effects of presence of cell on medium resistance change is ignorable: $R_s \approx R_{s0}$).

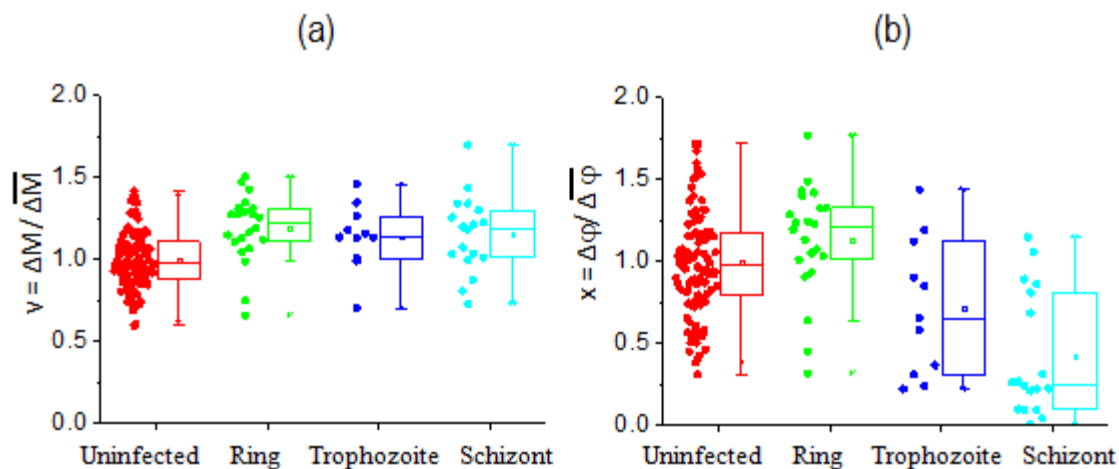


Fig.S2 (a) Scatter plot of normalized magnitude transition for uninfected RBCs and *Pf*-iRBCs in 0.5% w/v BSA-PBS. (b) Scatter plot of normalized phase transition for uninfected RBCs and *Pf*-iRBCs in 0.5% w/v BSA-PBS.

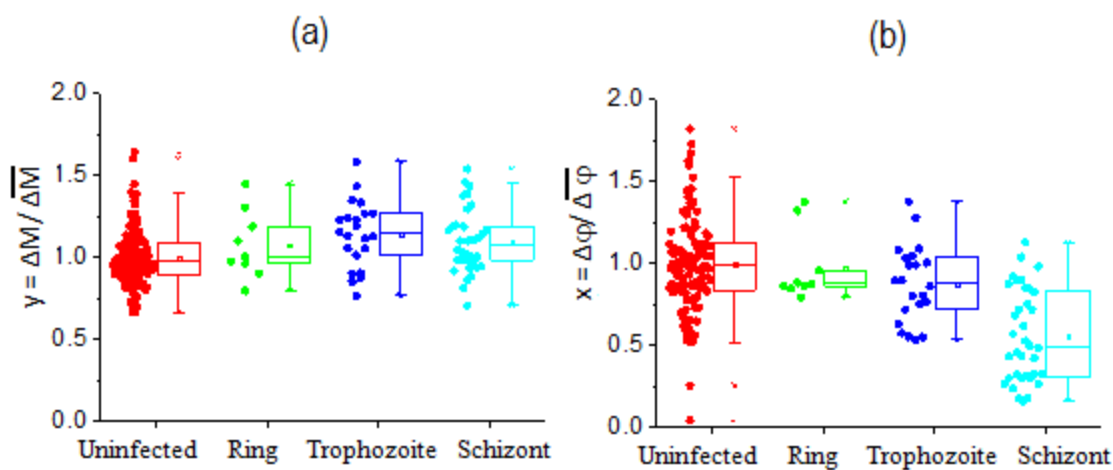


Fig.S3 (a) Scatter plot of normalized magnitude transition for uninfected RBCs and *Pf*-iRBCs in 1% w/v BSA-PBS. (b) Scatter plot of normalized phase transition for uninfected RBCs and *Pf*-iRBCs in 1% w/v BSA-PBS.

Supplementary Tables

Table S1 Descriptive statistics of EI transitions of individual cells for different BSA concentrations (N: uninfected RBCs; R: ring stage; T: trophozoite stage; S: schizont stage).

Condition EI transition	0.2 % w/v BSA-PBS			0.5% w/v BSA-PBS			1 % w/v BSA-PBS		
	Population (count)	Mean	S.D.	Population (count)	Mean	S.D.	Population (count)	Mean	S.D.
Mag (Ω)	N (120)	379.92	43.48	N (120)	385.27	81.15	N (120)	458.58	133.75
Pha (rad)		-0.13	0.03		-0.12	0.03		-0.24	0.13
Mag (Ω)	R (9)	433.33	43.19	R (22)	450.87	78.05	R (15)	660.40	126.70
Pha (rad)		-0.14	0.03		-0.12	0.03		-0.25	0.06
Mag (Ω)	T (22)	459.34	65.10	T (13)	451.36	84.38	T (16)	684.38	121.56
Pha (rad)		-0.13	0.05		-0.09	0.03		-0.21	0.07
Mag (Ω)	S (36)	505.22	92.98	S (26)	403.48	113.91	S (11)	408.69	68.19
Pha (rad)		-0.11	0.07		-0.05	0.02		-0.13	0.14

Table S2 Statistical significance of detection parameters for uninfected RBCs and *Pf*-iRBCs in 0.2% w/v BSA-PBS (N: uninfected RBCs; R: ring stage; T: trophozoite stage; S: schizont stage).

Offset δ				Normalized magnitude transition Y			Normalized phase transition X				
P-value	R	T	S	P-value	R	T	S	P-value	R	T	S
N	1.27E-07	1.08E-08	5.09E-06	N	2.79E-04	1.94E-04	1.17E-03	N	4.13E-01	9.12E-01	5.00E-01
R		5.88E-04	1.09E-04	R		1.99E-01	3.29E-02	R		5.44E-01	3.35E-01
T			4.63E-03	T			1.76E-01	T			5.90E-01

Table S3 Statistical significance of detection parameters for uninfected RBCs and *Pf*-iRBCs in 0.5% w/v BSA-PBS. (N: uninfected RBCs; R: ring stage; T: trophozoite stage; S: schizont stage).

Offset δ				Normalized magnitude transition Y			Normalized phase transition X				
P-value	R	T	S	P-value	R	T	S	P-value	R	T	S
N	1.25E-07	1.21E-04	1.60E-06	N	4.43E-04	4.65E-02	1.64E-04	N	1.06E-01	5.21E-02	3.71E-06
R		1.17E-02	1.20E-04	R		5.08E-01	6.30E-01	R		1.11E-02	4.10E-07
T			4.94E-02	T			8.50E-01	T			6.71E-02

Table S4 Statistical significance of detection parameters for uninfected RBCs and *Pf*-iRBCs in 1% w/v BSA-PBS. (N: uninfected RBCs; R: ring stage; T: trophozoite stage; S: schizont stage).

Offset δ				Normalized magnitude transition Y			Normalized phase transition X				
P-value	R	T	S	P-value	R	T	S	P-value	R	T	S
N	1.34E-01	3.17E-07	1.36E-08	N	3.06E-01	4.93E-03	8.96E-03	N	7.58E-01	3.46E-02	2.42E-11
R		9.22E-02	7.85E-03	R		4.41E-01	7.99E-01	R		2.67E-01	1.87E-04
T			7.12E-02	T			4.09E-01	T			2.38E-05